Industry Science and Engineering Vol. 3 No. 8, 2026

Lithium-ion Battery SOC Estimation under Broad-Range Temperatures and Time-Varying Operating Scenarios Using a Modified SR-UKF

Dan Zou
College of Mechanical and Electrical Engineering, Yunnan Opening University, Kunming, Yunnan, China

Abstract: The State-of-Charge (SOC) constitutes a vital state indicator for the battery management system of power lithium-ion batteries. Reliable State-of-Charge calculation provides prerequisites for safeguarding secure running of electrified automobiles and advancing onboard power allocation strategies. Faced with frequent model deviation, deteriorated computing precision and poor numerical robustness existing within power lithium-ion battery SOC algorithms across broad-range temperatures and time-varying operating scenarios, this work investigates SOC calculation schemes for power lithium-ion batteries that adapt to such complex thermal and operational circumstances. Based on the public LG-18650-HG2 dataset, the least-squares method is adopted for offline identification of model parameters, and a parameter-fitting correction model coupled with temperature and SOC is established. To overcome the limitations of the conventional square-root unscented Kalman filter, such as fixed noise statistics and weak robustness under complicated operational environments, the Sage-Husa adaptive noise strategy is introduced. A modified square-root unscented Kalman filter is mathematically derived to realize dynamic updating of process and measurement noise covariance. This work completes a full set of theoretical designs covering battery modeling, parameter fitting and filter algorithm improvement. Theoretical analysis demonstrates that the modified algorithm can cope with model disturbances arising from broad-range temperatures and time-varying operating scenarios, effectively suppress calculation errors triggered by abrupt working-condition shifts, and exhibits theoretical feasibility for high-accuracy SOC calculation. The present work offers theoretical insights toward developing state-calculation algorithms suited to power lithium-ion batteries in complicated operational environments.

Keywords: SOC Estimation; Wide-Temperature-Range Parameter Identification; Square Root Unscented Kalman Filter; Sage-Husa Adaptive Noise

1. Introduction

For power lithium-ion batteries, the State-of-Charge (SOC) acts as a pivotal state indicator within the battery management system (BMS) and serves as the fundamental basis for safety control, energy scheduling and power regulation of battery systems. Trustworthy SOC calculation helps to sustain reliable running of power lithium-ion battery systems, boost driving-range prediction precision, prolong battery service life and optimize onboard energy management, a feature that delivers considerable engineering and academic value for the industrial deployment of electrified vehicles [1].

Conventional approaches for SOC calculation cover the open-circuit voltage (OCV) technique, ampere-hour integration approach, filtering-driven algorithms and fundamental intelligent computing strategies. Nevertheless, under real-world automotive operation scenarios, power lithium-ion batteries confront complex surroundings marked by broad thermal swings and dynamic disturbances from time-varying working scenarios. Chemical traits of power lithium-ion batteries exhibit strong susceptibility toward thermal variations. Extreme high and low temperatures directly alter internal resistance within battery cells, triggering nonlinear shifts in critical metrics including polarization capacitance, available battery capacity, and open-circuit voltage [2]. Meanwhile, operating condition transitions including acceleration,

deceleration, idling and regenerative braking during driving subject batteries to dynamic disturbances such as high-rate charge-discharge, abrupt current changes and violent load fluctuations, which trigger dynamic polarization responses and result in instantaneous fluctuation of power battery parameters [3].

When dealing with broad thermal swings and time-varying working scenarios, conventional SOC calculation approaches reveal prominent limitations. Most model parameter calibrations are completed at ambient temperature, while extreme thermal conditions give rise to model deviation and magnified SOC calculation deviations. The ampere-hour integration method suffers from accumulated current sampling errors. Filtering-driven algorithms adopt static noise parameters and fail to accommodate time-varying operational shifts, which hinders real-time capture of abrupt changes in battery internal states. In addition, frequent operational transitions trigger sharp variations in battery dynamic features. Such behavior further enlarges discrepancies between model outputs and real cell properties, decelerating SOC calculation convergence and raising dynamic biases.

Temperature drift and operating condition disturbance do not act independently, but form coupled interference in multiple dimensions. The battery response characteristics under the same rate condition differ greatly between high and low temperature environments. Estimation strategies suitable for room temperature cannot cope with the combined scenario of extreme temperature ranges and drastic variable operating conditions. Most traditional estimation methods adopt fixed-parameter design and cannot dynamically adjust variables such as filter noise and model polarization parameters according to real-time temperature and operating conditions. Therefore, they can hardly adapt to battery state variations under complex coupled scenarios and exhibit poor universality and generalization ability [4].

This work puts forward a calculation scheme for power-battery SOC built upon a modified square-root unscented Kalman filter, targeting broad-range temperatures and time-varying operating scenarios. A power battery equivalent circuit simulation model that considers both wide-temperature and variable-condition dynamic characteristics is established, and an improved SR-UKF algorithm with adaptive noise adjustment and state correction is designed. This newly-developed solver strengthens anti-interference performance and cross-scenario adaptability for conventional SOC calculation approaches when facing extreme thermal zones and dynamic perturbation circumstances.

2. Characteristic Analysis of Power Lithium-ion Battery

2.1 Working Mechanism of Lithium-ion Battery

A lithium-ion cell mainly comprises a positive electrode, graphite-based negative electrode, organic electrolyte, separator and current collectors. Regarded as a rocking-chair intercalation and deintercalation cell, it achieves electrical energy storage and release through reversible transfer of lithium ions between the positive and negative electrodes.

In the charging phase, lithium ions are extracted from the active materials of the positive electrode. These ions pass through the electrolyte and separator toward the negative electrode and become embedded within graphite interlayers. At the same time, electrons travel from the positive electrode to the negative electrode along the external circuit; electrical energy is thereby transformed into chemical energy for storage.

When discharging, lithium ions embedded in the negative electrode are released. They move through the electrolyte to the positive electrode and intercalate into the crystal lattice of positive electrode materials. Electrons flow from the negative electrode to the positive electrode via the external circuit, and chemical energy is converted into electric power to supply external loads.

The electrochemical reaction formulas for positive and negative electrodes during charge and discharge processes are given in Equations (1) and (2).

$$LiMO_2 \leftrightarrow Li_{x-1}MO_2 + xLi^+ + xe^- \quad (1)$$

$$xLi^+ + xe^- + 6C \leftrightarrow Li_xC_6 \quad (2)$$

During the operation of lithium-ion batteries, all dynamic errors, polarization and temperature effects originate from the limited migration rate of lithium ions, which constitutes the fundamental source of SOC estimation errors.

2.2 Variation Law of Battery Electrical Characteristics under Wide Temperature Range

The core electrical parameters of lithium-ion batteries include internal resistance, effective

capacity, polarization voltage, etc. Temperature variation changes electrolyte viscosity, solid-phase diffusion coefficient of lithium ions and interfacial charge transfer rate, leading to obvious nonlinear drift characteristics of battery parameters [5].

(1) Temperature Drift Characteristic of Internal Resistance

A battery's overall internal resistance comprises two components: ohmic resistance and polarization resistance, and this parameter exhibits pronounced nonlinear characteristics as temperature varies. In the room-temperature range (20~40 ℃), the ion transport and electrochemical reaction conditions inside the cell are optimal, while the internal resistance stays at a low level with mild fluctuations. At low temperatures, the electrolyte viscosity rises and the charge transfer reaction rate drops; this phenomenon leads to a simultaneous sharp rise in both ohmic and polarization resistance. Under high-temperature conditions, the internal resistance decreases slightly over a short period.

(2) Temperature Drift Characteristic of Effective Capacity

The nominal capacity of a cell refers to its rated capacity under standard ambient temperature operating conditions, whereas the actual usable capacity is strongly affected by temperature. Under cold thermal conditions, lithium-ion solid-phase diffusion encounters barriers, and the available discharge capacity of the cell undergoes substantial attenuation. Elevated temperatures can moderately boost ion diffusion capability and produce a slight increase in short-term usable capacity. Nevertheless, prolonged operation at high temperatures triggers irreversible capacity fading of the cell and undermines the capacity benchmark for SOC calculation.

(3) Temperature Drift Characteristic of Polarization Voltage

The total polarization voltage of power cells consists of ohmic polarization, charge-transfer polarization and concentration polarization. Under low-temperature conditions, the polarization voltage corresponding to identical charge–discharge currents rises markedly. The terminal voltage of the cell deviates substantially from its equilibrium open-circuit voltage, accompanied by drastic dynamic voltage fluctuations. At ambient temperature, the polarization effect remains weak and stable, and the voltage response can precisely track variations in cell states. The polarization voltage drops marginally under high-temperature conditions.

Figure 1 illustrates the thermal drift behaviors of cell internal resistance, usable capacity and polarization voltage.

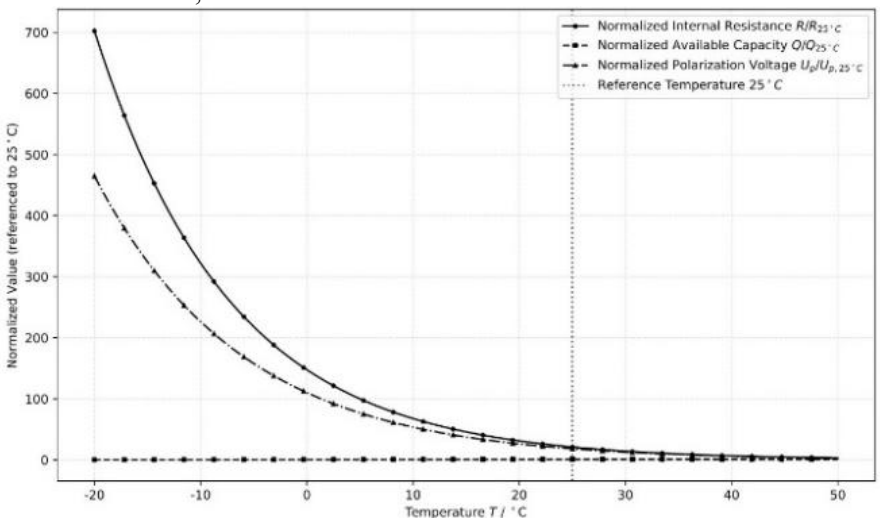


Figure 1. Normalized Drift Characteristics of Internal Resistance, Effective Capacity and Polarization Voltage of Lithium-ion Batteries under Wide Temperature Range

2.3 Dynamic Response Characteristics of Batteries under Variable Operating Conditions

Compared with the steady-state conditions with constant current in laboratory environments, vehicle variable operating conditions feature strong randomness of current, frequent abrupt changes and alternating positive/negative current rates. The dynamic polarization effect of the battery is continuously excited, and the electrical response exhibits strong nonlinearity and obvious hysteresis characteristics.

When abrupt operating condition changes such as

rapid acceleration, hill climbing and regenerative braking occur in vehicles, the battery is subjected to instantaneous high-rate impulse current. The dynamic current shock triggers instantaneous step change of battery terminal voltage and polarization accumulation effect.

Meanwhile, frequent switching of operating conditions produces remarkable polarization hysteresis and relaxation characteristics. During vehicle operation, discharge driving and charge regenerative conditions alternate frequently, leading to instantaneous reversal of lithium-ion migration direction. However, the lithium-ion concentration gradient inside the electrode solid phase and the interfacial polarization state are hysteretic; they cannot dissipate or reconstruct instantaneously with the abrupt change of current direction. Within a short period after condition switching, the battery still retains the residual polarization effect of the previous operating condition, resulting in a relaxation phenomenon that "SOC remains unchanged while voltage continuously varies". This disrupts the mapping relationship between terminal voltage and SOC and causes dynamic inaccuracy. Such polarization hysteresis is further amplified under wide temperature ranges. At low temperatures, the ion diffusion rate decreases greatly and the polarization relaxation time is significantly prolonged. The dynamic deviation after operating condition switching becomes more prominent, which seriously affects the state observation accuracy of the filtering algorithm [6,7].

The time-varying rules of load current, polarization voltage and terminal voltage under variable operating conditions are shown in Figure 2. The load current can undergo step-like abrupt changes, whereas the polarization voltage and terminal voltage show obvious hysteresis effects. The polarization relaxation phenomenon is prominent after condition switching, reflecting the dynamic evolution process of charge transfer and concentration polarization inside the battery.

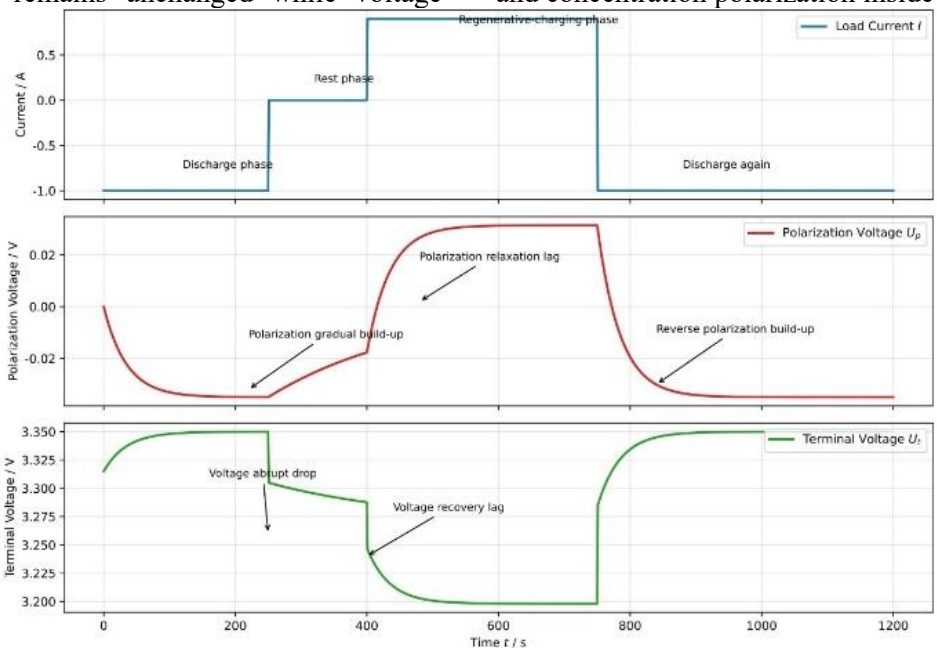


Figure 2. Dynamic Response Characteristics of Batteries under Variable Operating Conditions

The polarization hysteresis caused by dynamic current impact and operating condition switching is the main factor leading to degraded SOC estimation accuracy and state tracking lag under dynamic operating conditions.

3. Selection and Improvement of Power Battery Equivalent Circuit Model

Multiple equivalent circuit topologies have been applied for cell SOC calculation, such as the Thevenin model, PNGV model, first-order RC model and second-order RC model. Featuring a good trade-off between model complexity and dynamic fitting precision, the second-order RC model is well suited for vehicle-side SOC calculation under broad temperature ranges and frequent working condition transitions [8]. Accordingly, this work selects the second-order RC equivalent circuit as its fundamental modeling framework.

3.1 Construction of Second-Order RC Equivalent Circuit Model for Wide Temperature and Variable Operating

Conditions

Figure 3 presents the second-order RC equivalent circuit topology for power cells.

In the figure, $U_{ocv}(SOC,T)$ denotes the open-circuit voltage source; $R_0(T)$ represents the ohmic internal resistance. The first RC branch consisting of $R_1(T)$and $C_1(T)$ characterizes the fast charge-transfer polarization. The second RC branch with$R_2(T)$and $C_2(T)$ describes the slow concentration polarization. R_0, R_1, C_1, R_2 and C_2 are all functions of SOC and temperature T, instead of fixed values obtained at room temperature.

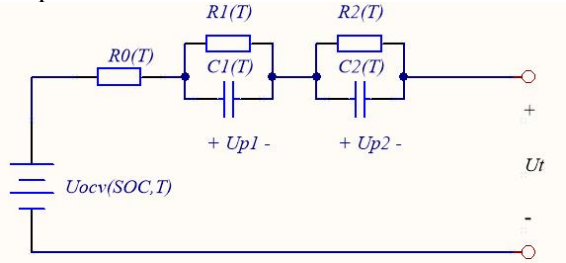


Figure 3. Second-order RC Equivalent Circuit Model

Kirchhoff's laws are employed to derive the state-space formulas for this topology, as provided in Equation (3).

$$\begin{cases} \dot{U}_{p1} = -\frac{1}{R_1C_1}U_{P1} + \frac{1}{C_1}I \\ \dot{U}_{p2} = -\frac{1}{R_2C_2}U_{P2} + \frac{1}{C_2}I \\ U_t = U_{OCV}(SOC,T) - IR_0 - U_{P1} - U_{P2} \end{cases} \quad (3)$$

where$U_{P1}$is the fast polarization voltage, U_{P2} is the slow polarization voltage, Symbol I represents the cell's charge and discharge current, where positive values correspond to discharge and negative ones to charging, and$U_t$represents the battery terminal voltage.

3.2 Analysis of Temperature Coupling Relationship of Model Parameters

R_0, R_1, C_1, R_2, C_2 and U_{ocv} in the second-order RC model have a strong coupling relationship with temperature. Under low-temperature conditions, the ohmic internal R_0 resistance increases exponentially as temperature decreases, the polarization resistances R_1 and R_2 rise significantly, the polarization time constants increase, and the polarization relaxation process slows down. Under high-temperature conditions, the ohmic internal resistance R_0 decreases slightly, the polarization resistances R_1 and R_2 decrease, speeding up the polarization response rate.

Parameter drift with temperature is the fundamental source of model mismatch under wide temperature ranges. It is necessary to establish the parameter-temperature mapping relationship to realize dynamic updating of model parameters with operating temperature and mitigate the model mismatch problem caused by wide temperature ranges [9].

3.3 Offline Identification and Temperature Correction of Model Parameters

Parameter settings largely determine the simulation precision of this second-order RC circuit topology. Parameters including R_0, R_1, C_1, R_2 and C_2 in the model are jointly affected by SOC and temperature. The parameter set identified at a single temperature cannot be directly applied to wide-temperature-range simulation. In this section, a simulation experimental scheme with multiple temperature gradients and multiple SOC intervals is designed. The least squares method is adopted to complete offline identification of model parameters under various operating conditions [10]. Furthermore, a temperature-parameter fitting correction model is constructed to realize adaptive updating of model parameters under different temperature conditions, which provides an accurate model foundation for the subsequent improved square root unscented Kalman filter algorithm.

3.3.1 Dataset selection and experimental operating condition analysis

In this paper, the publicly available measured dataset of LG-18650-HG2 lithium-ion battery from Mendeley is adopted for research. This dataset was tested and released by the Kollmeyer research team at McMaster University, Canada [11]. The test specimen is a fresh LG-18650-HG2 NMC cylindrical cell rated at 3.0 Ah nominal capacity and 3.6 V nominal voltage, with its charge cutoff limit set to 4.2 V and discharge cutoff limit at 2.5 V.

The dataset contains four groups of measured temperatures: 0 ℃, 10 ℃, 25 ℃ and 40 ℃, covering the typical low-temperature, room-temperature and high-temperature operating ranges of vehicle-mounted batteries. It also includes vehicle dynamic driving cycle data such as UDDS and US06, which can be used for variable-condition verification of the subsequent SOC estimation algorithm.

The public dataset does not provide measured HPPC data under the extremely low temperature of −20 ℃. To achieve the research objective of wide temperature range, this paper establishes a temperature-SOC coupled fitting model using

parameter samples identified from 0 ℃ to 40 ℃. The model parameters at −20 ℃ are obtained by extrapolation via the fitting model. Furthermore, the time-series data of HPPC profile at −20 ℃ are generated by simulation to supplement the extremely low-temperature samples. It should be noted that the data at −20 ℃ are derived from fitting extrapolation and simulation without support from physical measurement experiments. Meanwhile, all experiments are carried out on single cells, and the influence of cell inconsistency after battery pack assembly is not considered. The limitations of this part of data will be discussed in subsequent chapters.

3.3.2 Offline identification of battery model parameters based on least squares method

First, the continuous differential equation in Equation (3) is discretized to establish the difference form suitable for identification. The discrete state equation is obtained as shown in Equation (4).

$$\begin{cases} U_{p1,k+1} = \left(1 - \frac{T_s}{R_1 C_1}\right) U_{p1,k} + \frac{T_s}{C_1} I_k \\ U_{p2,k+1} = \left(1 - \frac{T_s}{R_2 C_2}\right) U_{p2,k} + \frac{T_s}{C_2} I_k \\ U_{t,k} = U_{ocv}(SOC_k) - I_k R_0 - U_{p1,k} - U_{p2,k} \end{cases} \quad (4)$$

where: k is the discrete sampling instant; T_s denotes the sampling time; I_k represents the loop current at time k; $U_{t,k}$ is the model output terminal voltage; $U_{ocv}(SOC_k)$ is the open-circuit voltage corresponding to the current SOC. The LG-18650-HG2 dataset is adopted as the source for parameter identification. The measured current series from this dataset serves as the model input, while the collected cell terminal voltage acts as the system observation quantity. Using the minimum sum of squared residuals as the identification criterion, the objective function for least squares parameter estimation is established [12], as given in Equation (5).

$$J = \sum_{k=1}^{N} (\widehat{U}_{t,k} - U_{t,k})^2 \rightarrow min \quad (5)$$

Where $\widehat{U}_{t,k}$ is the measured terminal voltage from the dataset, $U_{t,k}$ is the terminal voltage calculated and output by the second-order RC model, and N is the total number of sampling points in this segment. A set of model parameters R_0, R_1, C_1, R_2 and C_2 at this temperature-SOC operating point can be obtained by solving with the least squares algorithm.

All temperature and SOC operating points in the dataset are traversed, and parameter identification of each operating condition segment is completed sequentially to obtain multiple discrete parameter sample sets $(T_i, SOC_j, R_0(i,j), R_1(i,j), C_1(i,j), R_2(i,j), C_2(i,j))$. The root mean square error (RMSE) is introduced as the evaluation index for identification performance, and abnormal identification samples with excessive fitting error are eliminated, as shown in Equation (6).

$$RMSE = \sqrt{\frac{1}{N}\sum_{k=1}^{N} (\widehat{U}_{t,k} - U_{t,k})^2} \quad (6)$$

3.3.3 Construction of temperature-SOC coupled parameter fitting and correction model

According to the analysis of parameter identification results, the model parameters are simultaneously affected by the dual coupling effect of temperature and SOC and exhibit obvious nonlinear characteristics. Cell internal resistance exhibits an exponential trend against thermal changes, whereas SOC introduces polynomial parameter variations. Therefore, an exponential-polynomial combined form is adopted for resistance fitting [13], as shown in Equation (7).

$$R(T, SOC) = (a_0 + a_1 SOC + a_2 SOC^2) \cdot \exp\left(\frac{a_3}{T + 273.15}\right) \quad (7)$$

where R stands for R_0, R_1 and R_2; a_0, a_1, a_2, a_3 are the fitting coefficients to be solved.

C_1 and C_2 are fitted by the bivariate polynomial, as shown in Equation (8).

$$C(T, SOC) = b_0 + b_1 T + b_2 SOC + b_4 T^2 + b_4 SOC^2 + b_5 T \cdot SOC \quad (8)$$

Where b_0 sim b_5 are the fitting coefficients to be solved.

With the identified discrete parameter samples treated as reference fitting values, all corresponding fitting coefficients including R_0, R_1, C_1, R_2 and C_2 are calculated to minimize the residual sum of squares between fitted responses and the identified parameter set.

Since the public LG-18650-HG2 dataset lacks HPPC test data under the extremely low temperature of −20 ℃, the established temperature-SOC coupled fitting model is extrapolated to −20 ℃ to solve for the second-order RC model parameters corresponding to different SOC values at −20 ℃. The parameters at −20 ℃ are extrapolated results of the model, exceeding the temperature boundary of the original experiments. They cannot be verified by measured experimental data and are only used for subsequent algorithm simulation comparison.

The obtained fitting and correction model is

embedded into the second-order RC equivalent circuit model. At each step of the simulation calculation, the temperature and SOC at the current moment are read and substituted into the fitting function to update $R_0(T,SOC), R_1(T,SOC), R_2(T,SOC), C_1(T,SOC)$ and $C_2(T,SOC)$ in real time. Fixed room-temperature parameters are no longer adopted. This realizes adaptive matching of model parameters under wide temperature ranges and alleviates the problem of model mismatch caused by different temperatures.

4. Design of Improved SR-UKF Algorithm Adapted to Wide-Temperature and Variable Operating Conditions

Built upon the characteristic analysis of power cells, this work develops a temperature-SOC coupled second-order RC circuit topology, completes parameter identification and temperature fitting correction, and introduces an adaptive noise update scheme to establish a modified SR-UKF algorithm suitable for variable working scenarios under broad thermal ranges.

4.1 Principles of Standard Unscented Kalman Filter and Square Root Unscented Kalman Filter

The equivalent circuit model of power batteries belongs to nonlinear systems. Extended Kalman filtering (EKF) serves as a common tool for state estimation tasks. EKF will produce truncation errors in strongly nonlinear regions. By replacing local linearization with the unscented transform, the unscented Kalman filter can effectively avoid inherent errors caused by linear truncation [14].

The Unscented Transform (UT) picks deterministic sigma sample points such that their mean and covariance match the statistical properties of the initial state distribution. Once these sample points pass through the nonlinear mapping function, weighted statistical calculation yields the mean and covariance of states after nonlinear transformation.

The Sigma sampling formula is shown in Equation (9).

$$\begin{cases} X_0 = \bar{x} \\ X_i = \bar{x} + \sqrt{(n+\lambda)P_x)_i}, i = 1,2,...,n \\ X_{i+n} = \bar{x} - \sqrt{(n+\lambda)P_x)_i}, i = 1,2,...,n \end{cases} \quad (9)$$

Where x is the n-dimensional random variable, $\bar{x}$ denotes the mean value of the variable, $(\sqrt{\cdot})_i$ represents the covariance matrix, $\lambda = \alpha^2(n+k)-n$ is the i-th column of the matrix square root, and f is the scaling parameter.

The calculations of the corresponding mean weights and covariance weights are shown in Equation (10).

Here, α governs how far sample points spread, while β incorporates prior knowledge regarding the state distribution. Generally, β=2 is adopted under the Gaussian distribution condition.

$$\begin{cases} \omega_0^{(m)} = \frac{\lambda}{n+\lambda} \\ \omega_0^{(c)} = \frac{\lambda}{n+\lambda}(1+\alpha^2+\beta) \\ \omega_i^{(m)} = \omega_i^{(c)} = \frac{1}{2(n+\lambda)}, i = 1,2,...,2n \end{cases} \quad (10)$$

The conventional Unscented Kalman Filter (UKF) forwards sigma samples across nonlinear state and observation equations. Weighted statistical operations on these propagated samples then produce the state mean and covariance after nonlinear mapping. Iterative prediction and updating are implemented to achieve estimations for state variables including SOC.

The difference between the Square Root Unscented Kalman Filter (SR-UKF) and this modified algorithm's core feature is to propagate the square-root factor S of the covariance matrix rather than directly handling covariance P, satisfying $P = SS^T$. In the iteration process, Cholesky decomposition and QR decomposition are employed to update the square-root matrix, so as to avoid the negative definiteness problem of the covariance matrix.

The detailed execution procedures for this modified SR-UKF algorithm are outlined below.

(1) Decompose the initial covariance matrix P_0 via Cholesky factorization, yielding the initial square-root matrix $S_0 = chol(P_0)$;

(2) Sigma samples are generated from the state estimate together with square-root matrix S_{k-1};

(3) Time update and measurement update: propagate Sigma points through the state function and calculate the prior state estimate; update $S_{k|k-1}$ via QR decomposition; substitute Sigma points into the measurement equation to calculate the measurement prediction; compute the Kalman gain and residuals, and then obtain the posterior square root matrix $S_{k|k}$ by Cholesky rank update.

(4) Iteration: output $\hat{x}_{k|k}$, set k=k+1, then go back to Step 2 to create sigma samples and proceed into the next iteration.

4.2 Improved Square Root Unscented Kalman Filter Algorithm for Wide-Temperature and

Variable Operating Conditions

When SR-UKF is employed for power cell SOC estimation, noise matrices Q and R remain constant values. Across broad thermal domains and dynamic operating scenarios, cell internal resistance and polarization capacitance shift as temperature changes. Fixed noise parameters fail to accommodate dynamically varying model errors over the full temperature span, which weakens the system's robustness.

To solve the above problem, an adaptive noise covariance strategy is introduced to improve the SR-UKF algorithm.

4.2.1 Discrete State-Space Model of Power Battery

Based on the previously derived temperature-SOC coupled second-order RC circuit topology, the system state vector is defined in Equation (11).

$$x_k = [SOC_k, U_{p1,k}, U_{p2,k}]^T \quad (11)$$

Here, SOC_k represents the cell state of charge at sampling time k, while $U_{p1,k}$ and $U_{p2,k}$ stand for polarization voltages corresponding to the two RC branches.

The discrete state equation is expressed as shown in Equation (12).

$$\begin{cases} SOC_{k+1} = SOC_k - \frac{\Delta t}{C_N} I_k \\ U_{p1,k+1} = U_{p1,k} \exp\left(-\frac{\Delta t}{R_1 C_1}\right) + I_k R_1 [1 - \exp\left(-\frac{\Delta t}{R_1 C_1}\right)] \\ U_{p2,k+1} = U_{p2,k} \exp\left(-\frac{\Delta t}{R_2 C_2}\right) + I_k R_2 [1 - \exp\left(-\frac{\Delta t}{R_2 C_2}\right)] \end{cases} \quad (12)$$

The measurement equation is shown in Equation (13).

$$U_{t,k} = U_{ocv}(SOC_k, T_k) - I_k R_0 - U_{p1,k} - U_{p2,k} \quad (13)$$

Where Δt is the sampling time, C_N is the available capacity of the battery, I_k is the charge-discharge current, and U_{ocv} is the battery open-circuit voltage, which is a function of SOC and temperatureT_k. R_0, R_1, C_1, R_2 and C_2 adopt the temperature-SOC fitting parameters obtained in Section 3.3.3; extrapolated parameters are used for the low-temperature operating condition of −20 ℃.

4.2.2 Improved adaptive noise covariance strategy based on sage-husa

To address the problem of fixed noise matrices in the standard SR-UKF, the Sage-Husa adaptive idea [15] is adopted. The system innovation residual is adopted to update process noise Q_k and observation noise R_k online, enabling adaptive tuning of noise matrices under changing thermal and operating conditions.

The innovation residual, also known as observation residual, is shown in Equation (14).

$$e_k = U_{t,k} - \hat{U}_{t,k|k-1} \quad (14)$$

Residual covariance estimation is established, and a forgetting factor b is incorporated to regulate the weight assigned to historical data. This parameter takes values within the interval from 0.95 to 0.98.

The measurement noise update is shown in Equation (15).

$$R_k = (1-b)R_{k-1} + b[e_k e_k^T - S_{\hat{z},k|k-1} S_{\hat{z},k|k-1}^T] \quad (15)$$

The process noise matrix is shown in Equation (16).

$$Q_k = (1-b)Q_{k-1} + b[K_k e_k e_k^T Q_k^T] \quad (16)$$

Under broad thermal ranges and dynamic operating scenarios, the adaptive noise matrix can quantify the level of model mismatch in real time based on voltage residuals, automatically tune noise matrices and modify weights of the Kalman gain, thereby mitigating the impact of model deviations upon SOC prediction outcomes.

The adaptive SR-UKF algorithm based on Sage- Husa takes the current I_k, terminal voltage $U_{t,k}$ and battery temperature T_k at time k as input signals, and loads the temperature- SOC parameter mapping relationship simultaneously.

The algorithm is implemented in the following steps:

(1) Define the initial state $\hat{x}_0$, carry out Cholesky factorization for the initial covariance matrix and derive its square-root term S_0 ; initialize Q_0 and R_0, and specify forgetting factor b alongside upper and lower limits for noise terms.

(2) Read the current temperature and call the fitting function to update R_0, R_1, C_1, R_2, C_2 and U_{ocv}. under the current temperature and SOC.

(3) Generate Sigma sampling points based on $\hat{x}_{k-1|k-1}$ and S_{k-1}.

(4) Propagate Sigma points through the state equation to calculate the prior state estimate $\hat{x}_{k|k-1}$; update the prior square-root matrix $S_{k|k-1}$ via QR decomposition to complete the time prediction.

(5) Substitute Sigma points into the measurement equation to obtain the measurement prediction and calculate the square-root matrix of measurement prediction.

(6) Compute the observation residual e_k , perform Sage-Husa adaptive update to correct Q_k and R_k, and carry out threshold limiting.

(7) Calculate the Kalman gain and complete the measurement update. Obtain the posterior square-root matrix $S_{k|k}$ by Cholesky rank update, and output the state estimate $\hat{x}_{k|k}$

including the SOC estimation result at instant k.
(8) Set k=k+1, jump to Step 2 and proceed to the iteration of the next instant.
Figure 4 visualizes the workflow of this adaptive SR-UKF variant.

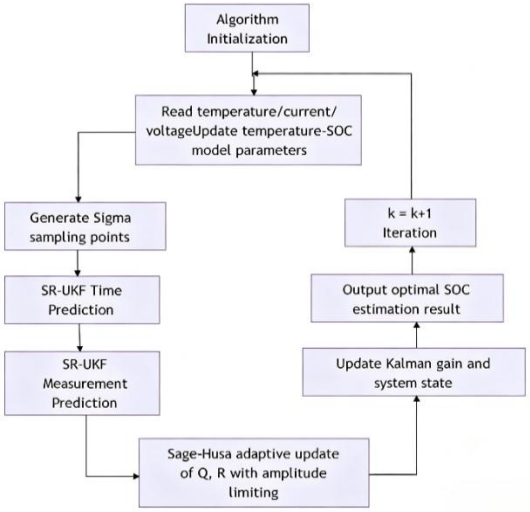


Figure 4. Flowchart of the Adaptive SR-UKF Algorithm

5. Conclusions and Prospects

This work targets high-precision SOC prediction for power lithium-ion cells across broad thermal ranges and dynamic operating scenarios as its research objective. Aiming at the problems including battery parameter drift, model mismatch and degraded SOC estimation accuracy of power batteries under high/low temperature environments and complex vehicle variable operating conditions, the operating principles of power cells and the evolution rules of their electrical features amid broad thermal ranges and dynamic working scenarios are analyzed. Building upon the above analysis, the second-order RC circuit topology is adopted as the fundamental model for state variable prediction. Based on the public LG-18650-HG2 dataset, the least squares method is adopted for offline identification of model parameters, and a temperature-SOC coupled parameter fitting correction model is established. Reasonable extrapolation of parameters is carried out under the extremely low temperature of −20 ℃ to characterize model parameters at different temperatures and SOC intervals. Meanwhile, the adaptive Sage-Husa noise framework is incorporated to construct this modified SR-UKF algorithm. It supports dynamic renewal of noise statistical properties and enhances the algorithm's adaptability against temperature drift and abrupt fluctuations in working scenarios.

This paper only completes theoretical modeling and derivation of algorithm improvement, and there are still some limitations in the research. The model parameters of the battery under the extremely low temperature of −20 ℃ are obtained by fitting and extrapolating the existing dataset rather than direct measurement and identification. In addition, physical experimental data are lacking to quantitatively verify the estimation accuracy, convergence characteristics and anti-interference ability of the improved SR-UKF algorithm. To address the two major limitations mentioned above, comprehensive measured cell datasets covering the entire temperature span will be collected in future research. These data will substitute fitted and extrapolated parameters, refine the temperature-SOC coupled model and raise the fidelity of the cell model. In parallel, a simulation framework or an experimental test bench for power cells will be established. Typical vehicle operating conditions such as DST and UDDS will be used to test the improved SR-UKF algorithm under multiple temperature conditions. Indicators including MAE, RMSE and convergence speed of the algorithm will be quantitatively evaluated to verify the practical estimation performance of the algorithm.

Acknowledgments

This paper is supported by Scientific Research Fund Project of Yunnan Open University, High-precision SOC Estimation of Power Batteries under Variable Working Conditions, Project No.: 25YNOU23.

References

[1] Wang Q Y, LI H. Safety issues and failure analysis of lithium batteries. New Energy Technology, 2021(11): 15-19.
[2] Wang M Z, XIAO Z L, ZHENG Y J. Sensitivity analysis of model parameters for lithium iron phosphate batteries at different temperatures. Journal of University of Shanghai for Science and Technology, 2022, 44(05): 449-456.
[3] Jiang J C, SUN B X. Lithium-ion battery modeling and state estimation. Beijing: China Machine Press, 2021.
[4] Chang S S. Research on modeling and state estimation of lithium-ion batteries under wide temperature range. Shanghai: Shanghai University of Electric Power, 2023.
[5] Li X Y. Research on model construction and

SOC estimation method of vehicle lithium-ion batteries. Harbin: Northeast Forestry University, 2025.
[6] Zhang Z. Research on Accurate State of Temperature Estimation Method for Vehicle Lithium-ion Batteries under Full Temperature and Full Life Cycle. Kunming University of Science and Technology, 2024.
[7] Xie Y, CHEN N, CHEN J, et al. Co-estimation of state of charge and model parameters for lithium-ion batteries based on variational Bayesian under time-varying noise and temperature conditions. Journal of Energy Storage, 2024, 96:112600.
[8] Chen D M. Research on modeling and SOC estimation method of lithium-ion batteries for electric vehicles. Jiaozuo: Henan Polytechnic University, 2023.
[9] Wang X D, DONG Z, WANG S H, et al. Wide-temperature and multi-condition SOC estimation of lithium-ion batteries based on improved open-circuit voltage model and adaptive square-root unscented Kalman filter. Transactions of China Electrotechnical Society, 2024, 39(24):7950-7964.
[10] Huangfu H W, HAN A C. Research on equivalent model establishment and parameter identification method of lithium battery. Electric Switchgear, 2020, 58(03): 37-41.
[11] Kollmeyer P, Vidal C, Naguib M, et al. LG 18650HG2 Li-ion Battery Data and Example Deep Neural Network xEV SOC Estimator Script. Mendeley Data, 2020. DOI:10.17632/cp3473x7xv.3.
[12] Fang J W. Research on Model Parameter Identification and State Estimation Method of Lithium Batteries. Yangzhou University, 2025.
[13] Du B H, ZHANG Y, WU T Z, et al. Online identification method for equivalent model parameters of echelon utilization lithium-ion batteries. Energy Storage Science and Technology, 2021, 10(01): 342-348.
[14] Julier S J, Uhlmann J K. Unscented filtering and nonlinear estimation. Proceedings of the IEEE, 2004, 92(3): 401-422.
[15] Lu J T, PENG Z R. Structural response reconstruction with improved Sage-Husa Kalman filter based on adaptive window length. Chinese Journal of Computational Mechanics, 2025, 42(2):212-220.